Journal of Marine Systems 192 (2019) 42–50

Contents lists available at ScienceDirect

Journal of Marine Systems

journal homepage: www.elsevier.com/locate/jmarsys

Sinking particle flux and composition at three sites of different annual sea ice cover in the Amundsen Sea, Antarctica

Minkyoung Kim[a], Eun J. Yang[b], Dongseon Kim[c], Jin-Hyun Jeong[c], Hyung J. Kim[c], Jisoo Park[b], Jinyoung Jung[b], Hugh W. Ducklow[d], SangHoon Lee[b], Jeomshik Hwang[a,*]

[a] School of Earth and Environmental Sciences, Research Institute of Oceanography, Seoul National University, Seoul 08826, South Korea
[b] Korea Polar Research Institute, Incheon 21990, South Korea
[c] Korea Institute of Ocean Science & Technology, Busan 49111, South Korea
[d] Lamont-Doherty Earth Observatory, Columbia University, Palisades, NY 10964, USA

ARTICLE INFO

Keywords:
Particulate organic carbon
Biological pump
Perennial ice-covered area
Polynya
Amundsen Sea

ABSTRACT

This study examines the sinking particle flux and composition of samples collected at three sites in the western Amundsen Sea, Antarctica: a perennial sea-ice-covered area, the central region of the Amundsen Sea polynya, and close to the Dotson Ice Shelf within the polynya. Time series sediment traps were deployed for one year at depths of 400–500 m from February and March 2012. Observations from the three sites confirm previously reported findings that the majority of annual POC (particulate organic carbon) flux in the Amundsen Sea occurs during the austral summer, with much smaller POC fluxes during other seasons. In the perennial ice-covered area, sea ice diatoms were the dominant source of sinking particles. In this region, the summertime POC flux is similar to that in the central polynya. However, the POC flux exhibited large interannual variability, with the reduction in sea ice cover and sufficient insolation being critical to enhanced sinking POC flux. Within the Amundsen Sea polynya, the sinking POC flux was higher in the central region than near the Dotson Ice Shelf, consistent with spatial variability in primary production. The site near the Dotson Ice Shelf had the lowest contribution of diatoms to sinking particles and the smallest POC flux among the three sites.

1. Introduction

The Amundsen Sea in the western Antarctic is experiencing rapid declining of sea ice cover and melting of ice shelves (Walker et al., 2007; Stammerjohn et al., 2012). If we are to determine how this region will respond to such changes it is critical to improve our understanding of the ecosystem properties and biogeochemistry of the Amundsen Sea. Because of a lack of field measurements, the biogeochemistry of the Amundsen Sea has been observed primarily using satellite telemetry (Arrigo and van Dijken, 2003; Arrigo et al., 2012). These studies showed that the Amundsen Sea polynya (ASP) in the western Amundsen Sea is the most productive polynya around Antarctica (Arrigo and van Dijken, 2003). Additionally, these polynyas provide environments that facilitate the uptake of atmospheric CO_2 (Arrigo et al., 2012).

The region north of the ASP is perennially covered with pack ice, even during summer (Stammerjohn et al., 2015). This region experiences a reduction in sea ice concentration during summer, but does not usually experience ice-free conditions. This perennial sea-ice-covered area is different from the "seasonal ice zone" (i.e., an area of ocean that extends from the permanent ice zone to the boundary where the winter sea ice extent is at a maximum). Perennial ice-covered regions around Antarctica cover 3–4 million km^2 in February compared with the full extent of 17–20 million km^2 in September (https://earthobservatory.nasa.gov). Therefore, it is important to understand primary production and particle export in the perennial ice-covered area.

Recent field campaigns have investigated the role of the biological pump in the Amundsen Sea (Arrigo and Alderkamp, 2012; Yager et al., 2012; Meredith et al., 2016; Yager et al., 2016; Lee et al., 2017). In situ measurements are limited to summer when access via icebreakers is possible. Moorings equipped with time series sediment traps facilitate the annual sampling of sinking particles, with the sinking particle flux providing a direct indication of POC export to the deeper water column.

The flux and biogenic composition of sinking particles was previously reported for two sites, one in the central ASP between December 18, 2010 and January 4, 2012 (Ducklow et al., 2015), and the other in the perennial ice-covered area north of the ASP between January 5, 2011 and January 5, 2012 (Kim et al., 2015). At both sites, an elevated

* Corresponding author.
E-mail address: jeomshik@snu.ac.kr (J. Hwang).

https://doi.org/10.1016/j.jmarsys.2019.01.002
Received 11 September 2018; Received in revised form 26 December 2018; Accepted 15 January 2019
Available online 18 January 2019
0924-7963/

flux of sinking particles was observed during summer, with particle flux remaining low during the other seasons. Peak POC flux in the ASP was roughly twice that in the perennial ice-covered area. Despite in situ primary production being higher in the ASP than in the perennial ice-covered area, POC fluxes at both sites were comparable when integrated over the summer (January and February 2011; Kim et al., 2015).

We expanded the available particle flux and composition dataset by collecting samples at three sites using sediment trap moorings deployed for one year. Building on the previous results, we investigated the following questions. 1) Is the high sinking POC flux in the perennial ice-covered area comparable to that in the center of the polynya a persistent feature? 2) How is POC flux in the perennial ice-covered area associated with the temporal evolution of sea ice? 3) Is spatial variability in satellite-based chlorophyll-*a* concentration within the ASP reflected in the sinking POC flux? 4) How does sinking particle composition vary spatially in the Amundsen Sea and how is this variability related to particle export?

2. Materials and methods

Time series sediment traps (McLane PARFLUX Mark 78G; conical type, aperture diameter = 80 cm with a height:diameter ratio of 2.5) were deployed on bottom-tethered hydrographic moorings at three sites (Fig. 1). Trapping efficiency of the conical type sediment traps has been debated. Regarding this issue, readers are referred to papers such as Buesseler et al. (2007, 2010). An RCM-11 current meter was deployed 2 m below each sediment trap (detailed information on mooring designs can be found in Ha et al., 2014). Station K1 is located in the northern part of the Amundsen Sea, which is mostly covered with perennial sea ice but experiences a reduction in sea ice concentration during summer. Sampling at Station K1 (72.40°S, 117.72°W, trap depth = 400 m, water depth = 530 m) was a continuation from the preceding year (Kim et al., 2015). Sinking particles were sampled from March 7, 2012 to March 16, 2013 (Table 1). Station K1 was originally visited in early February 2012; however, thick sea ice cover delayed the mooring turnaround until early March 2012, resulting in a data gap of about 60 days. Station K2 (73.28°S, 114.97°W, trap depth = 410 m, water depth = 830 m) is located in the central region of the ASP, which is characterized by high primary production (Yager et al., 2012). Samples were collected from February 15, 2012 to February 20, 2013. POC flux results at K2 are reported in Lee et al. (2017). Station K3 (74.19°S, 112.54°W; trap depth = 490 m, water depth = 1057 m) is located in front of the Dotson Ice Shelf. This region experiences low sea ice cover, even during winter (Stammerjohn et al., 2015), and primary production is lower than in the central region of the polynya (Yager et al., 2016). Samples were collected from February 17, 2012 to March 1, 2013. The sampling intervals were between 9 and 31 days, depending on the expected particle flux (Table 1). Each sample bottle was filled with filtered seawater collected from the trap depth, with sodium borate buffer and 10% formalin solution added as a preservative.

The samples were stored in a refrigerator at 2–4 °C. Upon inspection with the naked eye, any visible zooplankton specimens were removed using tweezers in a land-based laboratory. Each sample was split into five equal aliquots using a wet sample divider (WSD-10, McLane Laboratory). Three of the five equal aliquots were combined. This fraction was rinsed with ultrapure water (Milli-Q water) and the supernatant was removed after centrifugation. This process was repeated three times to remove salts and the residual formalin. The rinsed samples were then freeze dried and weighed for determination of total particle flux. The uncertainty of the particle flux determination is mainly from sample splitting and is < 5% (www.mclanelabs.com). One aliquot was used for radiocarbon analysis after rinsing with Milli-Q water and freeze drying. The other aliquot was used for microscopic examination of diatoms.

The dried samples were homogenized in an agate mortar prior to determination of total carbon, inorganic carbon, and biogenic opal content. The chemical analysis procedure is fully described in Kim et al. (2012). Briefly, total carbon content was determined using a Carlo-Erba 1110 CNS elemental analyzer with an analytical error of < 3% based on a sulfanilamide standard. Inorganic carbon content was measured using a UIC coulometrics carbon analyzer with an accuracy of > 98%. Organic carbon content was estimated as the difference between the total carbon and inorganic carbon contents. A conservative uncertainty of < 10% of the measured values was assigned for organic carbon content estimation. The biogenic opal content was determined following a wet alkaline extraction method with a precision of roughly 5% (DeMaster, 1981). For station K1, biogenic opal analysis was conducted only for the periods with a high particle flux (March to June 2012 and January to March 2013) due to the limited amount of samples available.

Radiocarbon isotope ratios were measured on a subset of samples (6 and 2 results for K2 and K3, respectively). Approximately 20 mg of finely ground particle samples were exposed to HCl fumes to remove inorganic carbon (Hedges and Stern, 1984; Komada et al., 2008) and combusted at 850 °C in closed quartz tubes. Cryogenically isolated CO_2 gas was analyzed for radiocarbon and stable carbon isotope ratios using standard techniques at the National Ocean Sciences Accelerator Mass Spectrometry facility at Woods Hole Oceanographic Institution (McNichol et al., 1994). The uncertainty associated with the $\Delta^{14}C$ measurements was < 10‰.

Particle samples were examined under the microscope for identification and quantification of diatom cells. Diatom enumeration was performed using a biological counting technique (Salter et al., 2012). A 1/5 aliquot of each sample was gently homogenized and 1–2 mL were drawn using a 5 mL standard pipette (ca. 1 cm of the tip was cut off to widen the mouth and thus minimize selective sampling of certain particle sizes) and diluted into a total volume of 20–50 mL of 0.2-mm-filtered preservative solution. The diluted sample was placed in a Sedgewick–Rafter counting chamber. Depending on diatom abundance, one quarter to one half of the chamber was examined with an inverted microscope with phase contrast (Olympus BX51) at 400× or 600× magnification. The uncertainty of cell counting was ~5% based on multiple analysis.

Sea ice concentration data were retrieved from the European Centre for Medium-Range Weather Forecasts (ECMWF) ERA-Interim reanalysis. We used the daily sea ice concentration with a horizontal resolution of 0.125° × 0.125°. Data were averaged over the regions (72.2–72.7°S, 118.4–117.4°W), (73.0–73.5°S, 115.5–114.5°W), and (74.0–74.25°S, 113.0–112.0°W) for Stations K1, K2, and K3, respectively. MODIS Aqua-derived estimates of surface chlorophyll-*a* concentration were obtained from the Goddard Space Flight Center. The data for the Amundsen Sea were available only between November and February because of low solar elevation and high sea ice cover. We used Level 3, 8-day composite global datasets with a spatial resolution of approximately 4.5 km. Primary production was estimated using the VGPM (vertically generalized production model) method (Behrenfeld and Falkowski, 1997) and MODIS data for the sea surface temperature, photosynthetically available radiation, and chlorophyll-*a*. To compare this data with the sinking POC flux at stations K2 and K3, primary production was estimated by averaging values over a larger region surrounding each station. Primary production was averaged over the regions (112–117°W, 73.0–73.5°S) for K2 and (111–114°W, between 73.75°S and the coast) for K3.

3. Results

3.1. Sea ice concentration and ocean currents

At K1, sea ice concentration reached minimum values of approximately 50% in February 2012 and 40% in March 2013 (Fig. 2a). Except during summer, sea ice concentration remained mostly over 90%.

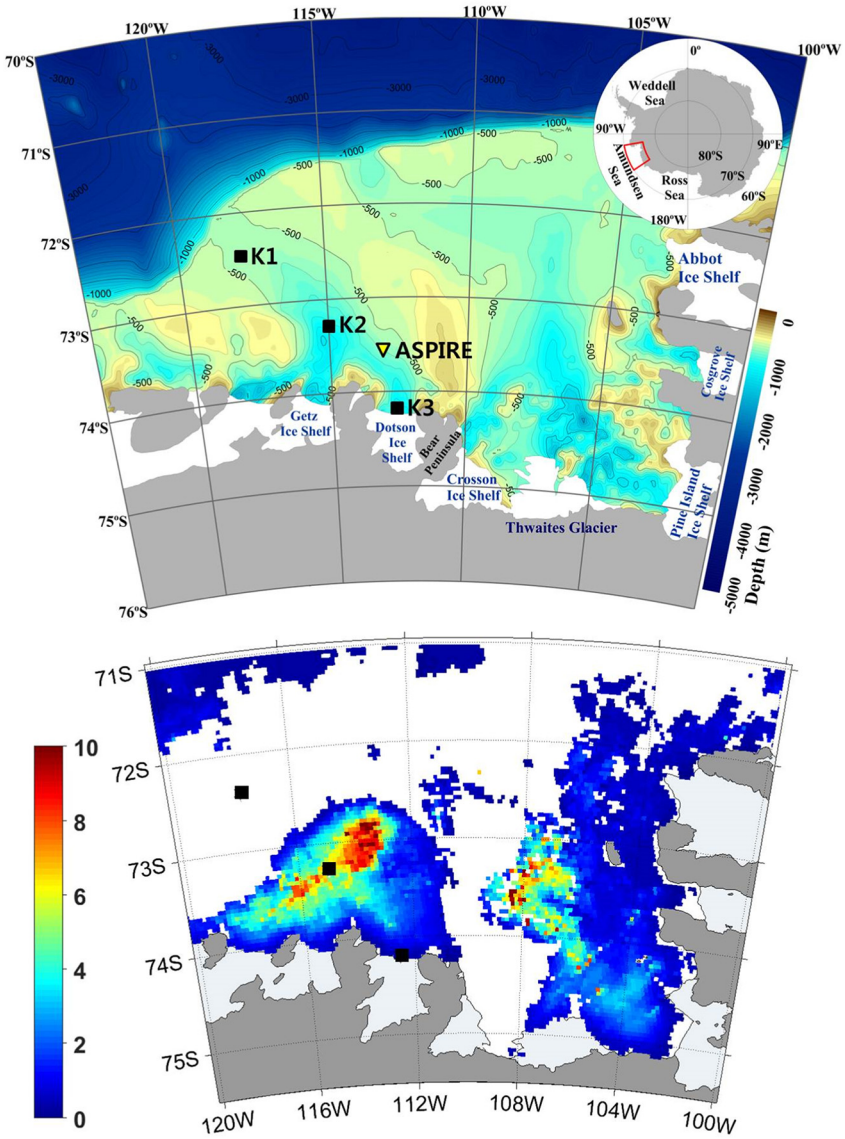

Fig. 1. (Top) Amundsen Sea bathymetry and the locations of sediment traps from this study (black squares) and the US Amundsen Sea Polynya International Research Expedition (ASPIRE) project (yellow downward-pointing triangle). (Bottom) Chlorophyll-*a* concentration derived from MODIS data (units of mg m^{-3}), averaged over January and February 2013 in the Amundsen Sea polynya (western side). The white region represents the perennial ice-covered area. (For interpretation of the references to colour in this figure legend, the reader is referred to the web version of this article.)

Therefore K1 remained in the perennial ice-covered area. At K2, located in the central polynya, minimum sea ice concentration was close to, or lower than 10% in February 2012 (Fig. 2b). The sea ice concentration started to decrease in early November 2012 and reached about 20% in late December. It recovered to around 70% briefly in early January 2013 and then decreased to the annual minimum in late February 2013. During the year, the surface characteristics of K2 changed from sea ice in winter, to marginal ice in spring, to open sea in summer – early fall. Station K3 was generally free of sea ice for more than three months during summer (Fig. 2c). This site was never fully covered with sea ice during the remainder of the year, with concentrations fluctuating between 30% and 80%.

The arithmetic mean of the current speed measured at 2 m below the trap at K1 was 5.7 ± 3.0 cm s^{-1}. Current direction varied with the integrated flow direction being northwestward (Fig. 3). At K2, the mean current speed was 5.9 ± 3.0 cm s^{-1}. Here, current direction varied widely with no predominant direction being evident. Integrated flow was southeastward. Current speed was somewhat higher at K3 than at the other stations, and speeds > 20 cm s^{-1} were recorded occasionally between July and October 2012. At K3, the mean current speed was 9.7 ± 5.6 cm s^{-1}, and the integrated current direction was northwestward. Considering the settling velocity of particles, estimated to be 10–100 m d^{-1} by McDonnell and Buesseler (2010), and the trap depths, we concluded that the collected biogenic particles originated from within a few tens of km of each site.

3.2. Flux, biogenic composition, and radiocarbon isotope ratio of sinking particles

Total particle flux at K1 ranged from 0.7 to 396 mg m^{-2} d^{-1}, with high values occurring during March and April 2012 (Fig. 2a). The particle flux was greatest at the beginning of the sampling period (March 2012) and decreased steadily to 16 mg m^{-2} d^{-1} in June. Low particle flux, ranging from 0.7 to 7.0 mg m^{-2} d^{-1}, persisted from July to December. Total particle flux increased slightly in January 2013 and fluctuated between 12 and 76 mg m^{-2} d^{-1} until the end of the sampling period on March 16. A prominent peak in particle flux, such as that recorded during the previous summer, was not observed. Total

Table 1
Sampling dates, fluxes, and compositions of biogenic particles at three sites in the Amundsen Sea. ND means not determined.

Sample no.	Cup opening date mm/dd/yy	Sampling interval days	Particle flux mg m^{-2}d^{-1}	POC flux mg C m^{-2}d^{-1}	TC%	POC%	TN%	Opal%	$CaCO_3$%	Δ^{14}C‰	Diatom flux 10^6 cells m^{-2}d^{-1}
Station K1											
1	3/7/12–4/1/12	25	396	25	6.6	6.3	0.84	70	2.8	ND	340
2	4/1/12–5/1/12	30	167	9.4	5.9	5.6	0.87	66	2.1	ND	160
3	5/1/12–6/1/12	31	59	3.8	6.6	6.3	1.0	52	2.4	ND	40
4	6/1/12–7/1/12	30	16	1.4	8.5	8.3	1.4	43	1.6	ND	7.8
5	7/1/12–8/1/12	31	2.5	0.7	26.8	26.8	5.1	ND	0.8	ND	0.19
6	8/1/12–9/1/12	31	2.4	0.7	30.7	28.8	5.8	ND	15	ND	0.09
7	9/1/12–0/1/12	30	3.3	0.7	23.5	21.3	4.0	ND	18	ND	0.15
8	10/1/12–11/1/12	31	3.2	0.5	15.0	14.1	2.3	ND	7.5	ND	0.075
9	11/1/12–11/16/12	15	0.7	ND	20.0	ND	2.4	ND	ND	ND	0.016
10	11/16/12–12/1/12	15	1.1	ND	17.9	ND	3.4	ND	ND	ND	0.046
11	12/1/12–12/10/12	9	3.4	ND	11.0	ND	1.7	ND	ND	ND	0.11
12	12/10/12–12/19/12	9	6.8	0.5	8.4	7.5	1.2	ND	7.9	ND	0.19
13	12/19/12–12/28/12	9	7.0	0.4	7.3	6.2	0.93	ND	9.0	ND	0.44
14	12/28/12–1/6/13	9	12	0.9	8.1	7.6	0.99	ND	4.0	ND	0.64
15	1/6/13–1/15/13	9	24	1.3	6.4	5.5	0.78	27	7.8	ND	3.9
16	1/15/13–1/24/13	9	36	1.9	5.8	5.2	0.67	31	4.7	ND	8.1
17	1/24/13–2/2/13	9	25	1.6	7.1	6.4	0.89	28	6.2	ND	9.2
18	2/2/13–2/11/13	9	36	2.2	7.7	6.3	0.84	30	12	ND	14
19	2/11/13–2/20/13	9	32	3.9	13.3	12.1	1.7	51	10	ND	23
20	2/20/13–3/1/13	9	17	1.3	7.2	7.2	0.99	ND	0.2	ND	16
21	3/1/13–3/16/13	15	76	4.7	6.8	6.2	0.90	38	5.0	ND	36
Station K2											
1	2/15/12–3/1/12	15	30	4.3	14.0	14.0	2.1	16	0.2	ND	3.7
2	3/1/12–3/16/12	15	15	3.5	23.5	23.4	3.9	20	0.8	ND	2.9
3	3/16/12–4/1/12	16	17	3.0	17.7	17.6	2.6	28	1.0	−175	3.9
4	4/1/12–5/1/12	30	3.9	0.7	17.9	17.8	3.0	ND	0.6	ND	0.45
5	5/1/12–6/1/12	31	54	3.2	6.1	6.0	0.82	19	1.1	−245	12
6	6/1/12–7/1/12	30	40	2.4	6.2	6.0	0.90	16	1.3	ND	5.5
7	7/1/12–8/1/12	31	42	2.5	6.0	5.8	0.79	14	1.2	−209	6.2
8	8/1/12–9/1/12	31	16	1.8	11.5	11.3	1.3	12	1.5	ND	0.88
9	9/1/12–10/1/12	30	65	2.8	4.7	4.4	0.59	12	2.5	ND	3.6
10	10/1/12–11/1/12	31	29	1.3	4.7	4.4	0.60	11	2.1	ND	1.3
11	11/1/12–11/16/12	15	40	1.5	4.0	3.7	0.47	10	2.4	ND	1.3
12	11/16/12–12/1/12	15	70	2.4	3.9	3.5	0.44	13	3.0	−240	1.9
13	12/1/12–12/10/12	9	87	4.8	5.8	5.5	0.85	16	2.1	ND	5.0
14	12/10/12–12/19/12	9	163	8.9	5.7	5.5	0.77	21	1.6	ND	14
15	12/19/12–12/28/12	9	179	10	5.7	5.6	0.74	21	1.3	−198	27
16	12/28/12–1/6/13	9	273	15	5.7	5.6	0.72	28	1.2	ND	55
17	1/6/13–1/15/13	9	222	13	6.1	6.0	0.87	28	1.4	ND	71
18	1/15/13–1/24/13	9	260	29	11.3	11.2	1.8	27	0.8	−171	69
19	1/24/13–2/2/13	9	4.1	0.5[a]	12.7	12.6[a]	1.8	ND	ND	ND	0.45
20	2/2/13–2/11/13	9	3.0	0.4[a]	14.7	14.6[a]	2.1	ND	ND	ND	3.6
21	2/11/13–2/20/13	9	4.7	0.7[a]	14.3	14.2[a]	2.2	ND	ND	ND	1.6
Station K3											
1	2/17/12–3/16/12	28	2.5	0.5	20.6	20.5	2.7	ND	1.2	ND	2.6
2	3/16/12–4/1/12	16	9.0	1.7	18.9	18.8	2.8	13	1.4	ND	4.7
3	4/1/12–5/1/12	30	8.5	0.9	11.2	11.1	1.9	15	1.2	ND	2.2
4	5/1/12–6/1/12	31	33	2.4	7.6	7.4	1.2	13	1.8	−224	7.4
5	6/1/12–7/1/12	30	26	1.4	5.5	5.3	0.84	9	1.5	ND	6.7
6	7/1/12–8/1/12	31	45	2.7	6.1	6.0	1.0	10	0.3	ND	9.6
7	8/1/12–9/1/12	31	14	0.9	6.5	6.1	1.1	5	3.3	ND	3.5
8	9/1/12–10/1/12	30	16	2.0	13.2	12.9	3.0	3	3.1	ND	1.2
9	10/1/12–11/1/12	31	8.4	0.5	6.6	6.3	1.1	6	2.6	ND	1.0
10	11/1/12–1/16/12	15	14	0.6	4.3	3.9	0.53	7	2.8	ND	1.1
11	11/16/12–12/1/12	15	25	1.5	6.4	5.9	1.1	6	4.6	ND	1.9
12	12/1/12–12/10/12	9	25	1.6	7.2	6.6	0.88	6	4.5	ND	2.3
13	12/10/12–12/19/12	9	79	3.2	4.5	4.1	0.62	7	3.2	ND	4.7
14	12/19/12–12/28/12	9	42	1.9	4.9	4.4	0.57	6	3.7	ND	5.2
15	12/28/12–1/6/13	9	47	3.4	7.7	7.2	0.98	5	4.3	ND	4.8
16	1/6/13–1/15/13	9	14	1.1	8.5	7.9	1.2	5	5.0	ND	2.1
17	1/15/13–1/24/13	9	162	16	10.0	9.8	1.4	11	2.2	−197	58
18	1/24/13–2/2/13	9	62	8.2	13.5	13.2	2.1	15	2.9	ND	26
19	2/2/13–2/11/13	9	24	3.8	16.7	16.0	2.6	14	6.2	ND	6.5
20	2/11/13–2/20/13	9	22	3.2	15.0	14.2	2.3	17	6.5	ND	7.6
21	2/20/13–3/1/13	9	22	3.1	15.1	13.9	2.1	12	11	ND	7.0

[a] These values are based on estimated POC content under the assumption that inorganic carbon content was 0.1%.

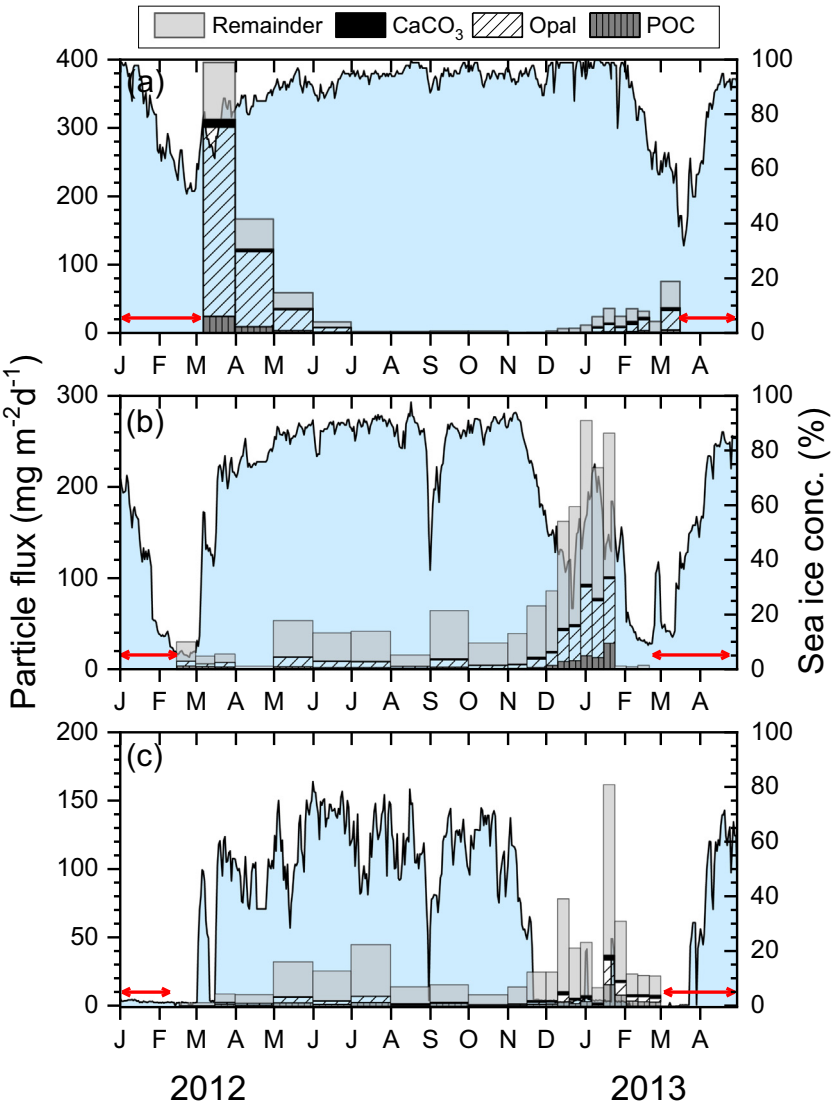

Fig. 2. Fluxes of each biogenic component (POC, $CaCO_3$, and opal,) and the remainder that is not accounted for by these components at stations (a) K1, (b) K2, and (c) K3. Tick marks on *x*-axis indicate the start of each month. Note that the *y*-axis scales are not equal. Horizontal arrows denote periods of no data. Sea ice concentration (blue shading) is represented on the right-hand *y*-axis. (For interpretation of the references to colour in this figure legend, the reader is referred to the web version of this article.)

particle flux at K2 ranged from 3.0 to 273 mg m^{-2} d^{-1} (Fig. 2b). Our sample collection, having started in mid-February, most probably missed the peak sinking particle flux during summer 2011–2012. Total particle flux remained low (3.9–70 mg m^{-2} d^{-1}) until November 2012, and then increased steadily to the maximum value in late December 2012 to early January 2013. The flux dropped to < 5.0 mg m^{-2} d^{-1} from January 24 to the end of the sampling period. We have not determined whether this sudden drop in particle flux was a sampling artifact, although we verified the functionality of the trap carousel (clogging of the funnel is a possibility). Total particle flux at K3 ranged from 2.5 to 162 mg m^{-2} d^{-1}. Temporal variability at K3 was similar to that at K2. A high particle flux was not observed in late February 2012, when sampling began. The flux was low during the winter until November, when the flux started to increase. The highest value was observed in late January 2013, after which the particle flux decreased rapidly.

The POC content at K1 ranged between 5.6% and 6.3% during the high particle flux period of March–May 2012 (Fig. 4), before increasing to high values (up to 29%) in July and August. POC content gradually decreased to about 14% in October 2012. Subsequently, the POC content during the summer generally remained low (5% to 8%). In contrast, higher values were observed at K2 in summer than in winter. The highest POC content of 23% was observed during the period February–April 2012. The values then remained between 3.5% and 6.0% (with an exception of 11% in August) until mid-January 2013, with values increasing to 14.6% during February 2013. At K3, both the temporal variability and magnitude of the POC content were similar to K2. The temporal variability of POC flux resembled that of total particle flux (Fig. 2). The POC flux varied within the ranges 0.4–25, 0.4–29, and 0.5–16 mg C m^{-2} d^{-1} at K1, K2, and K3, respectively. The sampling-duration-weighted average POC fluxes were 4.0, 3.8, and 2.1 mg C m^{-2} d^{-1}, which correspond to annual fluxes of 1.5, 1.4, and 0.78 g C m^{-2} yr^{-1} at stations K1, K2, and K3, respectively.

$CaCO_3$ accounted for 3.2% (based on annually integrated fluxes) of the particle flux at K1 (Fig. 4). The duration-weighted average $CaCO_3$ contents at both K2 and K3 (1.5% and 2.7%, respectively) were lower than that at K1. The $CaCO_3$ flux, with a maximum value of 11 mg m^{-2} d^{-1} at K1, accounted for the smallest portion of the mass flux and was almost insignificant at all sites (Fig. 4).

The biogenic opal content at K1 was the highest (70%) in March

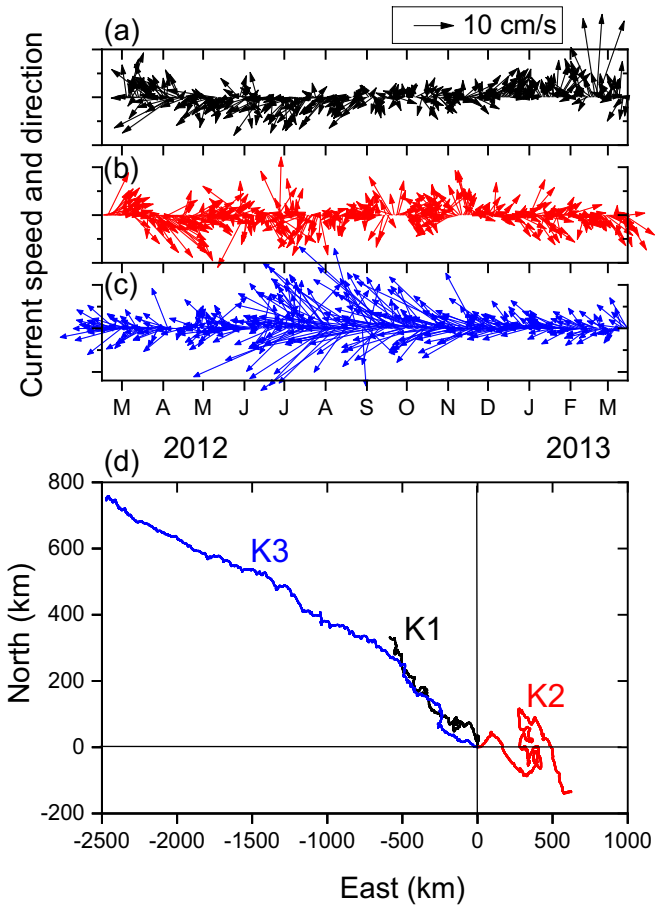

Fig. 3. Daily current speed and direction measured at 2 m below each trap at stations (a) K1, (b) K2, and (c) K3. (d) Progressive vector diagrams at three stations. The origin indicates the location on the initial day.

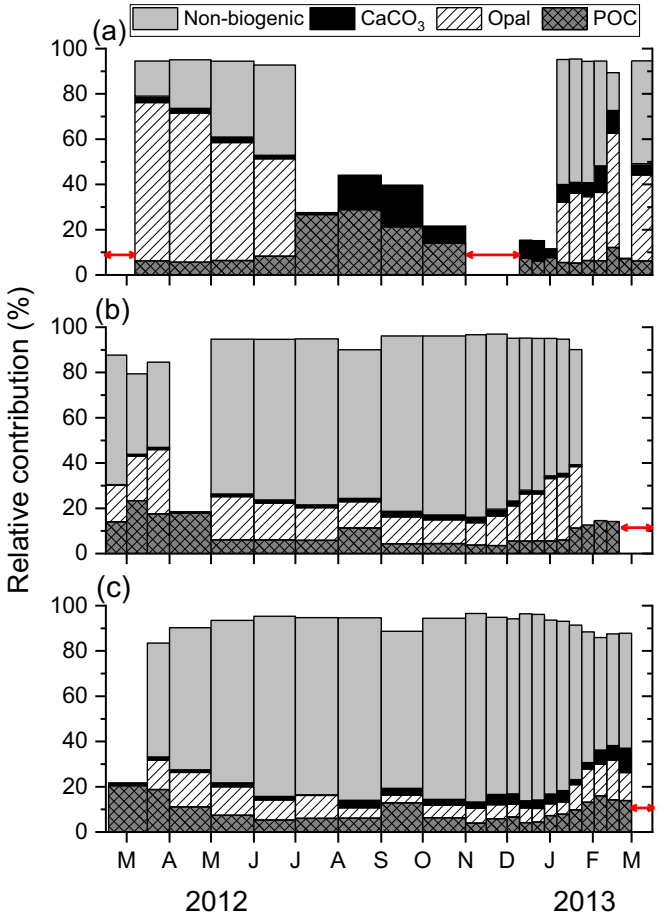

Fig. 4. Temporal variability in the relative contributions of each biogenic component and the non-biogenic component that is not accounted for by biogenic components (POC × 1.88, $CaCO_3$, and opal) at stations (a) K1, (b) K2, and (c) K3. Horizontal arrows denote periods of no data.

2012, before decreasing to 43% in June 2012 (Fig. 4). It increased from 27% in January to 51% in mid-February 2013. The biogenic opal flux at K1 ranged from 6.4 to 277 mg m^{-2} d^{-1} (note that opal data are not available for winter; Fig. 2). At K2, the biogenic opal content varied between 10% and 28%. The opal content started to increase in November 2012, reaching the highest values during January 2013. The biogenic opal flux ranged from 2.9 to 75 mg m^{-2} d^{-1} (Fig. 2). Among the three sites, the biogenic opal content and flux were lowest at K3, with the opal flux in the range 0.5–18 mg m^{-2} d^{-1}.

Non-biogenic material was estimated as the difference between the total mass and the sum of biogenic opal, $CaCO_3$, and POC × 1.88 (the ratio 1.88 for particulate organic matter over POC was adopted from Lam et al., 2011). The associated uncertainty is smaller than 10%. Non-biogenic material was dominant at K2 and K3, accounting for up to 80% of the particle flux (Fig. 4). Non-biogenic material flux was highest during summer at all sites, with the largest fluxes observed at K2 during December to January (Fig. 2).

The flux of diatom cells was highest at K1, especially in March and April 2012 (Fig. 5). The diatom flux remained low during winter and increased from January 2013 to the end of sampling in March at K1. However, the highest flux in March 2013 was an order of magnitude lower than that of March 2012. At K2 and K3, no prominent peaks in diatom flux were observed over the period February–April 2012. The diatom flux began to increase in December 2012, and peaked in January 2013, at both K2 and K3. The peak diatom flux occurred much earlier (> 1 month) at K2 and K3 than at K1.

Viewed under the microscope, the diatom assemblages at all sites were composed primarily of *Fragilariopsis cylindrus/curta, Thalassiosira, Chaetoceros,* and *Pseudonitzschia. Fragilariopsis cylindrus/curta* were the most abundant species (accounting for > 80% of the diatom assemblages) and were therefore primarily responsible for the observed temporal variability in the diatom fluxes. Diatoms did not contain chloroplasts. No hypnospores were observed.

The radiocarbon isotope ratio ($\Delta^{14}C$ values) at K2 ranged between −171‰ and −245‰, with higher values observed during summer (not shown, Table 1). At K3, the $\Delta^{14}C$ values observed in May 2012 and late-January 2013 were −224‰ and −197‰, respectively.

4. Discussion

4.1. Temporal evolution of sea ice and POC flux

Sea ice influences photosynthetically available radiation, primary production, and the dominant primary producers in the near-surface ocean (Smith Jr and Comiso, 2008; Smith Jr et al., 2014) and hence influences the magnitude and efficiency of particle export from the euphotic zone to the deep water column (Ramseier et al., 1999; Garrity et al., 2005). A model was developed to estimate the POC flux as a function of annual sea ice concentration for the seasonal ice zone (Garrity et al., 2005). This model estimated a low POC flux when the annual sea ice concentration was over 80% (< 1 g C m^{-2} yr^{-1}). Compared with this model, the annual POC flux at K1 was more than double the expected value at the corresponding sea ice concentration, emphasizing that the perennial ice-covered area behaves differently to the seasonal ice zone, in terms of POC export.

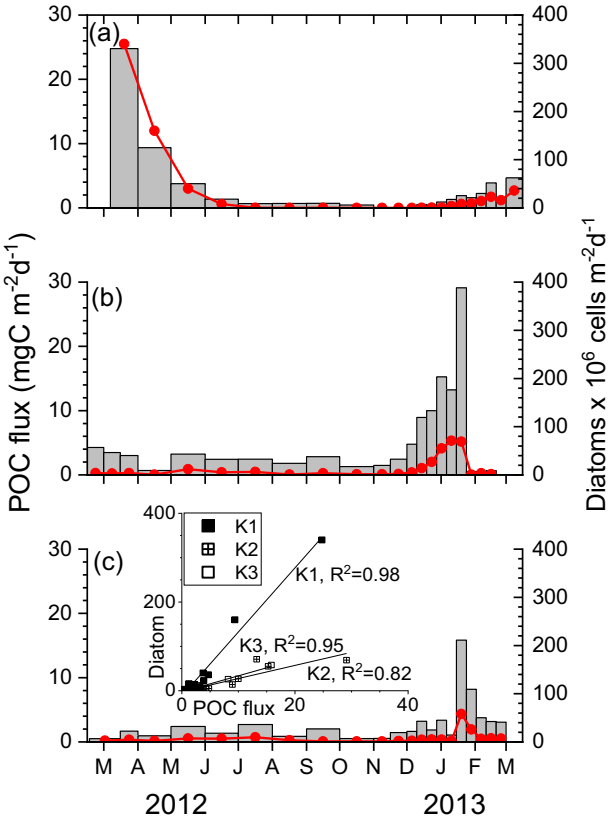

Fig. 5. Fluxes of POC (bars) and diatom cells (symbols) at Stations (a) K1, (b) K2, and (c) K3. The insert shows the relationship between diatom cell flux and POC flux. R^2 values are also shown for each site.

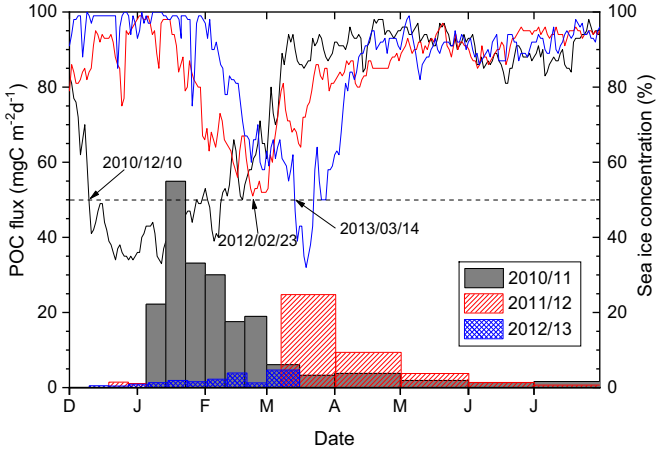

Fig. 6. Temporal variability of POC flux (bars) and sea ice concentration (lines) at station K1. The data are presented on a common time axis from December to July to show the variability during three summer and fall periods.

The summer POC flux exhibited high interannual variability at K1 (Fig. 6). For example, the prominent peak in January 2011 was not observed in January 2013. Also, the POC flux in March 2012 was larger than those in the other two years. The dominant diatoms, *Fragilariopsis cylindrus/curta*, are known as sea ice algae (Lizotte, 2001). Especially at K1, the water column species *Fragilariopsis kerguelensis* accounted for < 5% of the diatom community in the surface waters during the December 2013 to January 2014 cruise (Y.J. Lee, pers. comm.). Diatom cell flux and the POC flux at K1were tightly coupled (R^2 = 0.98, Fig. 5). POC content in diatoms cells, especially *Flagilariopsis spp.*, reportedly ranges between 128 and 158 pgC per cell (Cornet-Barthaux et al., 2007). When the diatom cell flux was converted to POC flux based on these values, the observed POC flux in March and April 2012 can be fully explained by diatom-derived POC flux.

The sea ice concentration was examined as the major parameter that affects POC production and flux in the perennial ice-covered area. To indicate when sea ice began to decline, we used the day when a 50% sea ice concentration was first reached, as has been used in other studies (e.g., Yager et al., 2016). In 2011, the highest POC flux occurred 34–44 days after the sea ice decline on December 10, 2010 (Fig. 6). During the following summer, sea ice concentration barely reached 50% on February 23, 2012. As sampling resumed on March 7 in the second year, after a hiatus of around 60 days, our sampling period may not have resolved the peak POC flux and may have occurred during the declining phase of the POC flux. However, if it took about 40 days from sea ice decline to phytoplankton bloom, as we observed during the preceding summer, and as was also observed by Yager et al. (2016), our first sample potentially measured the maximum POC flux. The POC flux of the first sample in March 2012 (24.8 mg C m^{-2} d^{-1}) was about half of the peak POC flux in January 2011 (54.9 mg C m^{-2} d^{-1}) (Fig. 6). The difference was also conspicuous when monthly-integrated values were compared (768 mg C m^{-2} $month^{-1}$ for March vs. 1140 mg C m^{-2} $month^{-1}$ for January). In 2013, the sea ice concentration reached 50% on March 14 and the POC flux increased until the end of the sampling period. Although diatom cell flux values over 20 million cells m^{-2} d^{-1} indicate that there was a phytoplankton bloom, the POC flux at the end of the sampling was much lower than those in the previous two summers. No data are available after mid-March 2013 to determine whether POC flux increased further or not.

Based on these short time series, the POC flux between December and April appears to be affected by the timing of sea ice reduction, both in terms of the time-integrated flux and peak magnitude. A probable explanation for the time delay between sea ice reduction and peak POC flux may be a “seeding hypothesis”, in which sea ice diatoms released to the water column from sea ice upon its melting, can stimulate subsequent blooms in the water column (Lizotte, 2001). In March 2013, sea ice melting occurred too late in the season, when insolation was diminishing, for a full-fledged bloom to occur. Our preliminary interpretation is that the timing of sea ice reduction, in addition to sea ice reduction itself, is important for a diatom bloom and enhanced POC export in the perennial ice-covered area. Therefore, although high POC flux comparable to that in the central ASP was observed at K1, similar high POC export cannot be equally expected across the perennial ice-covered area because of these restraints. The few locations that were examined under the perennial sea ice cover in the Amundsen Sea suggest low organic carbon accumulation rates compared with the ASP, further supporting this hypothesis (M. Kim et al., 2016). Ultimately, longer time series will be needed to establish a quantitative relationship between sea ice concentration and flux phenology.

4.2. Spatial variability in sinking particle flux and composition

The annual POC fluxes at stations K1 and K2 were similar; however, the composition of the biogenic particles was differed. The contribution of biogenic opal to the sinking particles was highest at K1, comprising 62% of the total flux for the period when data were available, compared with 20% and 9% at K2 and K3, respectively (Fig. 4). The biogenic-Si/POC ratio (wt/wt) was 2.8 at K1 compared with 1.2 at K2 and 0.46 at K3. The opal flux was derived mostly from diatoms, because radiolarians and silicoflagellates were seldom observed in the sinking particles. The ratio of diatom cell flux to POC flux was the highest at K1 (Fig. 5). Despite the varying contribution of diatoms to POC flux, the fluxes were tightly coupled at all stations (the insert of Fig. 5).

The difference in the sinking particle composition can be compared with the distinct phytoplankton compositions observed between the two regions in the upper 100 m layer during expeditions in January

2011 (Yang et al., 2016) and January 2014 (Lee et al., 2016b). Yang et al. (2016) reported that in January 2011, diatoms accounted for 90 ± 44% and 24 ± 10% of the total phytoplankton biomass, whereas *Phaeocystis antarctica (P. antarctica)* accounted for 2% and 73 ± 32% in the perennial ice-covered area and ASP, respectively. Similar spatial variability in the phytoplankton distribution was also observed based on pigment analysis during expeditions in February 2012 and January 2014 (Lee et al., 2016a).

While both sites were within the ASP, the POC flux at K3 was roughly half that at K2, reflecting the spatially-heterogeneous distribution of POC production. A different sampling depth at K3, ~80 m deeper than at K2, is not the major cause of the observed difference because the attenuation of POC flux from 410 m to 490 m is ~15% based on Martin curve (we used a *b* value of −0.8 and calculated the export production value that matches the observed flux at 490 m, after which we calculated the POC flux at 410 m using these values; Berelson, 2001; Martin et al., 1987). At K2, the diatom flux in December and the first half of January was significantly higher than at K3. During summer, when satellite data are available, chlorophyll-*a* concentrations in surface waters were several times higher in the central region of the ASP than on the periphery (Fig. 1b and also Mu et al., 2014; La et al., 2015). Average primary production from November 2012 through February 2013 was estimated to be 760 and 550 mg C m^{-2} d^{-1} for the regions including stations K2 and K3, respectively. The duration-weighted average sinking POC flux over the same period was 7.3 and 3.6 mg C m^{-2} d^{-1} at K2 and K3, respectively, resulting in an export and transfer efficiency (ratio of POC flux to primary production) of ~1% in the ASP.

We were not able to determine the export and transfer efficiency for K1 because no primary production data are available except for a snapshot. However, diatom-dominancy can affect the export and transfer efficiency of POC in favor of Station K1. The diatoms' relatively large volume and siliceous mineral content facilitate settling (Collier et al., 2000). McDonnell and Buesseler (2010) examined the particle size spectrum and their corresponding sinking velocities, finding that diatoms and krill fecal pellets had high sinking velocities across the size spectrum. Factors influencing the export efficiency in the ASP include slow sinking of *P. Antarctica*, (Dunbar et al., 1998; Asper and Smith Jr, 1999), and/or efficient remineralization due to prolonged exposure to microorganisms in the water column (Ducklow et al., 2015). Alternatively, *P. antarctica* may be channeled through the microbial food web via zooplankton grazing rather than contributing to vertical carbon flux (Reigstad and Wassmann, 2007; Hyun et al., 2016; Yang et al., 2016).

4.3. Contribution of non-biogenic particles

As the sampling sites were located on the continental shelf, the contribution from the lateral supply of allochthonous organic matter and lithogenic particles to the collected sinking particles was expected to be considerable. Radiocarbon analysis of the sinking particle samples collected during the preceding year in the perennial ice-covered area implied that the lateral supply of aged organic carbon could be a considerable source of POC, but only during the winter (Kim et al., 2015).

We used the non-biogenic material as a proxy for lithogenic particles. Non-biogenic material was the dominant component of the sinking particles, especially at K2 (62%, based on annually integrated fluxes, average flux = 41.0 mg m^{-2} d^{-1}) and K3 (68%, 19.0 mg m^{-2} d^{-1}), but was less prominent at K1 (19%, < 12 mg m^{-2} d^{-1}; note that an exact flux value was not calculated because there were no data for winter; Fig. 4). Sources of lithogenic material include aeolian dust deposition, sediment resuspension, and the melting of sea ice, icebergs, and ice shelves (Planquette et al., 2013). Deposition of aeolian dust in Antarctica's coastal regions is negligible compared with the observed non-biogenic material flux (Planquette et al., 2013). Although the K1 trap was the closest to the seafloor (ca. 130 m above the bottom), the total particle flux was extremely low from June to December, suggesting that local resuspension of sediment was not the major source. A much higher value at K2 compared with K1 and K3 suggest that lithogenic particles were released from sea ice melting. The higher non-biogenic material flux during summer compared with other seasons also implies that particles were released by sea ice melting. Fine particles were possibly scavenged more efficiently by the high flux of sinking particles in summer. Planquette et al. (2013) showed that particulate (> 5 μm) aluminum concentration was considerably higher (throughout the water column) in front of the Dotson Ice Shelf than at other locations. Aluminum concentration was especially high both near the seafloor and in the near-surface layer, suggesting two distinct sources of particulate aluminum (Planquette et al., 2013).

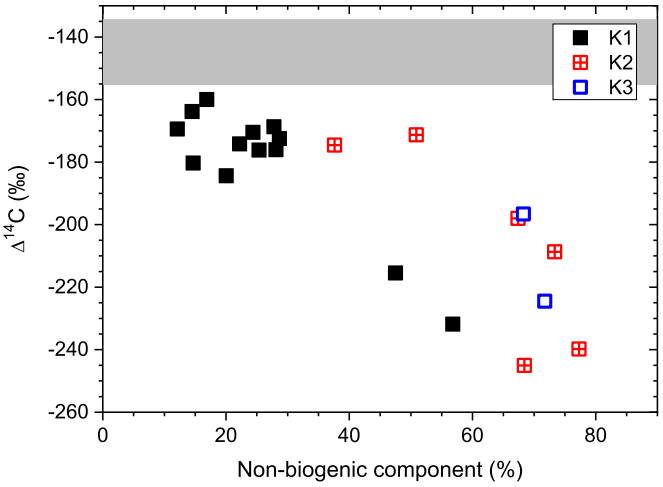

Fig. 7. Relationship between $\Delta^{14}C$ values of sinking POC and content of non-biogenic particles. Results from the preceding year at K1 are also shown for comparison (Kim et al., 2015). The shaded bar indicates the range of $\Delta^{14}C$ values of dissolved inorganic carbon in the study region (n = 4; B. Kim et al., 2016).

The $\Delta^{14}C$ values and the contents of the non-biogenic material in sinking particles were negatively correlated (Fig. 7). The $\Delta^{14}C$ values of dissolved inorganic carbon in surface water collected in 2012 from the study region ranged between −135‰ and −155‰ (n = 4; B. Kim et al., 2016). All observed values of sinking POC were lower than these values, indicating that the sinking POC contained aged POC from allochthonous sources. The $\Delta^{14}C$ values of surface sediments (0–1 cm, n = 4) in the Amundsen Sea ranged between −311‰ at a site near K2 in the ASP and − 418‰ near the Dotson Ice Shelf (M. Kim et al., 2016). Therefore, inclusion of resuspended sediments is a plausible explanation of the observed $\Delta^{14}C$ results. In addition, particles from the basal melting of icebergs and ice shelves may also supply aged POC. Exact sources of aged POC and the mode of delivery remain to be determined.

5. Summary

As observed in previous studies, the POC flux exhibited strong seasonal variability, with most of the annual POC flux occurring during the austral summer when the sea ice concentration was lowest. The ASP showed a high POC flux and is a key component of carbon cycling in the Amundsen Sea. However, the POC flux in the perennial ice-covered area, mostly supplied by sea ice diatoms, was high and comparable with the central region of the ASP, emphasizing the importance of the perennial ice-covered area to Amundsen Sea carbon cycling. However, the summer POC flux in the perennial ice-covered area exhibited high interannual variability. Both the reduction of sea ice cover and the timing when this reduction occurs are important: sea ice reduction in early summer for sufficient insolation appears to be crucial to maintaining high POC fluxes. Particle composition at the perennial ice-covered area

and the central ASP was different, reflecting the difference in the phytoplankton community at the two sites: primarily sea ice diatoms in the former and *P. antarctica* in the latter. The importance of the diatom-derived POC flux in the perennial ice-covered area was demonstrated by the biogenic-Si/POC ratio being more than double that in the central ASP. The periphery of the ASP near the Dotson Ice Shelf showed much a smaller particle flux than the center. Lower diatom fluxes especially in early summer, in addition to lower primary production, appear to be responsible for the observed difference in the POC flux.

Acknowledgments

We thank Sosul Cho at KIOST for the elemental analysis, Hyoung Sul La for providing sea ice data, and all cruise participants for their help with sampling, the captain and crew of the IBRV *Araon* for help at sea, and the staff at NOSAMS WHOI for radiocarbon analysis. This work was supported by the Korea Institute of Ocean Science and Technology (PN67330) and the Korea Polar Research Institute (PE18060). H. Ducklow was supported by NSF Award ANT 0839012.

References

Arrigo, K.R., Alderkamp, A.-C., 2012. Shedding dynamic light on Fe limitation (DynaLiFe). Deep-Sea Res. II 71, 1–4.
Arrigo, K.R., van Dijken, G.L., 2003. Phytoplankton dynamics within 37 Antarctic coastal polynya systems. J. Geophys. Res. 108 (27-21).
Arrigo, K.R., Lowry, K.E., van Dijken, G.L., 2012. Annual changes in sea ice and phytoplankton in polynyas of the Amundsen Sea, Antarctica. Deep-Sea Res. II 71-76, 5–15.
Asper, V.L., Smith Jr., W.O., 1999. Particle fluxes during austral spring and summer in the southern Ross Sea, Antarctica. J. Geophys. Res. 104, 5345–5359.
Behrenfeld, M.J., Falkowski, P.G., 1997. Photosynthetic rates derived from satellite-based chlorophyll concentration. Limnol. Oceanogr. 42, 1–20.
Berelson, W.M., 2001. The flux of particulate organic carbon into the ocean interior: a comparison of four US JGOFS regional studies. Oceanography 14, 59–67.
Buesseler, K.O., Antia, A.N., Chen, M., Fowler, S.W., Gardner, W.D., Gustafsson, O., Harada, K., Michaels, A.F., van der Loeff, M.R., Sarin, M., Steinberg, D.K., Trull, T., 2007. An assessment of the use of sediment traps for estimating upper ocean particle fluxes. J. Mar. Res. 65, 345–416.
Buesseler, K.O., McDonnell, A.M.P., Schofield, O.M.E., Steinberg, D.K., Ducklow, H.W., 2010. High particle export over the continental shelf of the west Antarctic Peninsula. Geophys. Res. Lett. 37, L22606.
Collier, R., Dymond, J., Honjo, S., Manganini, S., Francois, R., Dunbar, R., 2000. The vertical flux of biogenic and lithogenic material in the Ross Sea: moored sediment trap observations 1996–1998. Deep-Sea Res. II 47, 3491–3520.
Cornet-Barthaux, V., Armand, L., Quéguiner, B., 2007. Biovolume and biomass estimates of key diatoms in the southern ocean. Aquat. Microb. Ecol. 48, 295–308.
DeMaster, D.J., 1981. The supply and accumulation of silica in the marine environment. Geochim. Cosmochim. Acta 45, 1715–1732.
Ducklow, H.W., Wilson, S.E., Post, A.F., Stammerjohn, S.E., Erickson, M., Lee, S., Lowry, K.E., Sherrell, R.M., Yager, P.L., 2015. Particle flux on the continental shelf in the Amundsen Sea Polynya and western Antarctic peninsula. Elementa 3, 000046.
Dunbar, R.B., Leventer, A.R., Mucciarone, D.A., 1998. Water column sediment fluxes in the Ross Sea, Antarctica: atmospheric and sea ice forcing. J. Geophys. Res. 103, 30741–30759.
Garrity, C., Ramseier, R., Peinert, R., Kern, S., Fischer, G., 2005. Water column particulate organic carbon modeled fluxes in the ice-frequented Southern Ocean. J. Mar. Syst. 56, 133–149.
Ha, H.K., Wåhlin, A.K., Kim, T.W., S.H., L., Lee, J.H., Lee, H.J., Hong, C.S., Arneborg, L., Bjork, G., Kalen, O., 2014. Circulation and modification of warm deep water on the central Amundsen Shelf. J. Phys. Oceanogr. 44, 1493–1501.
Hedges, J.I., Stern, J.H., 1984. Carbon and nitrogen determinations of carbonate-containing solids. Limnol. Oceanogr. 29, 657–663.
Hyun, J.-H., Kim, S.-H., Yang, E.J., Choi, A., Lee, S.H., 2016. Biomass, production, and control of heterotrophic bacterioplankton during a late phytoplankton bloom in the Amundsen Sea Polynya, Antarctica. Deep-Sea Res. II 123, 102–112.
Kim, H.J., Hyeong, K., Yoo, C.M., Khim, B.K., Kim, K.H., Son, J.W., Kug, J.S., Park, J.Y., Kim, D., 2012. Impact of strong El Niño events (1997/98 and 2009/10) on sinking particle fluxes in the 10 °N thermocline ridge area of the northeastern equatorial Pacific. Deep-Sea Res. I 67, 111–120.
Kim, M., Hwang, J., Kim, H.J., Kim, D., Yang, E.J., Ducklow, H.W., La Hyoung, S., Lee, S.H., Park, J., Lee, S., 2015. Sinking particle flux in the sea ice zone of the Amundsen shelf, Antarctica. Deep-Sea Res. I 101, 110–117.
Kim, M., Hwang, J., Lee, S.H., Kim, H.J., Kim, D., Yang, E.J., Lee, S., 2016. Sedimentation of particulate organic carbon on the Amundsen shelf, Antarctica. Deep-Sea Res. II 123, 135–144.
Komada, T., Anderson, M.R., Dorfmeier, C.L., 2008. Carbonate removal from coastal sediments for the determination of organic carbon and its isotopic signatures, $\delta^{13}C$ and $\Delta^{14}C$: comparison of fumigation and direct acidification by hydrochloric acid. Limnol. Oceanogr. Methods 6, 254–262.
La, H.S., Lee, H., Fielding, S., Kang, D., Ha, H.K., Atkinson, A., Park, J., Siegel, V., Lee, S., Shin, H.C., 2015. High density of ice krill (Euphausia crystallorophias) in the Amundsen Sea coastal Polynya, Antarctica. Deep-Sea Res. I 95, 75–84.
Lam, P.J., Doney, S.C., Bishop, J.K., 2011. The dynamic ocean biological pump: insights from a global compilation of particulate organic carbon, $CaCO_3$, and opal concentration profiles from the mesopelagic. Glob. Biogeochem. Cycles 25, GB3009. https://doi.org/10.1029/2010GB003868.
Lee, Y.C., Park, M.O., Jung, J., Yang, E.J., Lee, S.H., 2016a. Taxonomic variability of phytoplankton and relationship with production of CDOM in the Polynya of the Amundsen Sea, Antarctica. Deep-Sea Res. II 123, 30–41.
Lee, Y., Yang, E.J., Park, J., Jung, J., Kim, T.W., Lee, S., 2016b. Physical-biological coupling in the Amundsen Sea, Antarctica: influence of physical factors on phytoplankton community structure and biomass. Deep-Sea Res. I 117, 51–60.
Lee, S., Hwang, J., Ducklow, H.W., Hahm, D., Lee, S.H., Kim, D., Hyun, J.H., Park, J., Ha, H.K., Kim, T.W., 2017. Evidence of minimal carbon sequestration in the productive Amundsen Sea Polynya. Geophys. Res. Lett. 44, 7892–7899.
Lizotte, M.P., 2001. The contributions of sea ice algae to Antarctic marine primary production. Am. Zool. 41, 57–73.
Martin, J.H., Knauer, G.A., Karl, D.M., Broenkow, W.W., 1987. VERTEX: carbon cycling in the northeast Pacific. Deep-Sea Res. I 34, 267–285.
McDonnell, A.M.P., Buesseler, K.O., 2010. Variability in the average sinking velocity of marine particles. Limnol. Oceanogr. 55, 2085–2096.
McNichol, A., Osborne, E., Gagnon, A., Fry, B., Jones, G., 1994. TIC, TOC, DIC, DOC, PIC, POC – unique aspects in the preparation of oceanographic samples for ^{14}C-AMS. Nucl. Instrum. Methods Phys. Res., Sect. B 92, 162–165.
Meredith, M.P., Ducklow, H.W., Schofield, O., Wåhlin, A., Newman, L., Lee, S., 2016. The interdisciplinary marine system of the Amundsen sea, southern ocean: recent advances and the need for sustained observations. Deep-Sea Res. II 123 (1–6).
Mu, L., Stammerjohn, S., Lowry, K., Yager, P., 2014. Spatial variability of surface pCO_2 and air-sea CO_2 flux in the Amundsen Sea Polynya, Antarctica. Elementa 2, 000036.
Planquette, H., Sherrell, R.M., Stammerjohn, S.E., Field, M.P., 2013. Particulate iron delivery to the water column of the Amundsen Sea, Antarctica. Mar. Chem. 153, 15–30.
Ramseier, R.O., Garrity, C., Bauerfeind, E., Peinert, R., 1999. Sea-ice impact on long-term particle flux in the Greenland sea's is Odden-Nordbukta region, 1985–1996. J. Geophys. Res. 104, 5329–5343.
Reigstad, M., Wassmann, P., 2007. Does Phaeocystis spp. contribute significantly to vertical export of organic carbon? Biogeochemistry 83, 217–234.
Salter, I., Kemp, A.E., Moore, C.M., Lampitt, R.S., Wolff, G.A., Holtvoeth, J., 2012. Diatom resting spore ecology drives enhanced carbon export from a naturally iron-fertilized bloom in the Southern Ocean. Glob. Biogeochem. Cycles 26, GB1014.
Smith Jr., W.O., Comiso, J.C., 2008. Influence of sea ice on primary production in the Southern Ocean: a satellite perspective. J. Geophys. Res. 113, C05S93.
Smith Jr., W.O., Ainley, D.G., Arrigo, K.R., Dinniman, M.S., 2014. The oceanography and ecology of the Ross Sea. Annu. Rev. Mar. Sci. 6, 469–487.
Stammerjohn, S., Massom, R., Rind, D., Martinson, D., 2012. Regions of rapid sea ice change: an inter-hemispheric seasonal comparison. Geophys. Res. Lett. 39, L0501.
Stammerjohn, S., Maksym, T., Massom, R., Lowry, K., Arrigo, K., Yuan, X., Raphael, M., Randall-Goodwin, E., Sherrell, R., Yager, P., 2015. Seasonal sea ice changes in the Amundsen Sea, Antarctica, over the period of 1979–2014. Elementa 3, 000055.
Walker, D.P., Brandon, M.A., Jenkins, A., Allen, J.T., Dowdeswell, J.A., Evans, J., 2007. Oceanic heat transport onto the Amundsen Sea shelf through a submarine glacial trough. Geophys. Res. Lett. 34, 1–4.
Yager, P.L., Sherrell, L., Stammerjohn, S., Alderkamp, A., Schofield, O., Abrahamsen, E., Arrigo, K., Bertilsson, S., Garay, D., Guerrero, R., 2012. ASPIRE: the Amundsen Sea Polynya international research expedition. Oceanography 25, 40–53.
Yager, P.L., Sherrell, R.M., Stammerjohn, S.E., Ducklow, H.W., Schofield, O.M.E., Ingall, E.D., Wilson, S.E., Lowry, K.E., Williams, C.M., Riemann, L., Bertilsson, S., Alderkamp, A.-C., Dinasquet, J., Logares, R., Richert, I., Sipler, R.E., Melara, A.J., Mu, L., Newstead, R.G., Post, A.F., Swalethorp, R., van Dijken, G.L., 2016. A carbon budget for the Amundsen Sea Polynya, Antarctica: estimating net community production and export in a highly productive polar ecosystem. Elementa 4, 00140.
Yang, E.J., Jiang, Y., Lee, S., 2016. Microzooplankton herbivory and community structure in the Amundsen Sea, Antarctica. Deep-Sea Res. II 123, 58–68.